

Research Paper

Imaging atherosclerotic plaques by targeting Galectin-3 and activated macrophages using (⁸⁹Zr)-DFO- Galectin3-F(ab')₂ mAb

Zohreh Varasteh¹✉, Francesco De Rose¹, Sarajo Mohanta^{2,4}, Yuanfang Li², Xi Zhang², Benedikt Miritsch^{3,4}, Giorgia Scafetta⁸, Changjun Yin^{2,4}, Hendrik B. Sager^{3,4}, Sarah Glasl^{5,6}, Dimitris Gorpas^{5,6}, Andreas J.R. Habenicht^{2,4}, Vasilis Ntziachristos^{5,6}, Wolfgang A. Weber¹, Armando Bartolazzi^{7,8}✉, Markus Schwaiger¹, Calogero D'Alessandria¹✉

1. Department of Nuclear Medicine, Klinikum rechts der Isar der TUM, Munich, Germany.
2. Institute for Cardiovascular Prevention, University Hospital of Ludwig-Maximilians-University, Munich, Germany.
3. Department of Cardiology, German Heart Center Munich, Munich, Germany.
4. Deutsches Zentrum für Herz-Kreislauf-Forschung (DZHK) e.V., partner site Munich Heart Alliance.
5. Institute of Biological and Medical Imaging, Helmholtz Zentrum München, Munich, Germany.
6. Chair of Biological Imaging and Center for Transnational Cancer Research (TranslaTUM), Technical University of Munich, Munich, Germany.
7. Pathology Research Laboratory, Cancer Center Karolinska, SE-17176 Stockholm, Sweden.
8. Pathology Research Laboratory, St. Andrea University Hospital, Rome, Italy.

✉ Corresponding authors: PD Calogero D'Alessandria, PhD. Department of Nuclear Medicine, Klinikum rechts der Isar der TUM, Ismaningerstrasse 22, 81675 Munich, Germany. E-mail: calogero.dalessandria@tum.de; Tel.: (+49) 89 4140 4579; Prof Armando Bartolazzi MD, Pathology Research Laboratory, St. Andrea University Hospital, via di Grottarossa 1035, 00189 - Rome, Italy. E-mail: armando.bartolazzi@ki.se; Tel.: (+39) 0633775321; Dr Zohreh Varasteh, Department of Nuclear Medicine, Klinikum rechts der Isar der TUM, Ismaningerstrasse 22, 81675 Munich, Germany. E-mail: zohreh.varasteh@tum.de; Tel.: (+49) 89 4140 6333.

© The author(s). This is an open access article distributed under the terms of the Creative Commons Attribution License (<https://creativecommons.org/licenses/by/4.0/>). See <http://ivyspring.com/terms> for full terms and conditions.

Received: 2020.07.03; Accepted: 2020.11.11; Published: 2021.01.01

Abstract

Rationale: The high expression of Galectin-3 (Gal3) in macrophages of atherosclerotic plaques suggests its participation in atherosclerosis pathogenesis, and raises the possibility to use it as a target to image disease severity *in vivo*. Here, we explored the feasibility of tracking atherosclerosis by targeting Gal3 expression in plaques of apolipoprotein E knockout (ApoE-KO) mice *via* PET imaging.

Methods: Targeting of Gal3 in M0-, M1- and M2 (M2a/M2c)-polarized macrophages was assessed *in vitro* using a Gal3-F(ab')₂ mAb labeled with AlexaFluor@488 and ⁸⁹Zr-desferrioxamine-thiourey-phenyl-isothiocyanate (DFO). To visualize plaques *in vivo*, ApoE-KO mice were injected *i.v.* with ⁸⁹Zr-DFO-Gal3-F(ab')₂ mAb and imaged *via* PET/CT 48 h post injection. Whole length aortas harvested from euthanized mice were processed for Sudan-IV staining, autoradiography, and immunostaining for Gal3, CD68 and α-SMA expression. To confirm accumulation of the tracer in plaques, ApoE-KO mice were injected *i.v.* with Cy5.5-Gal3-F(ab')₂ mAb, euthanized 48 h post injection, followed by cryosections of the body and acquisition of fluorescent images. To explore the clinical potential of this imaging modality, immunostaining for Gal3, CD68 and α-SMA expression were carried out in human plaques. Single cell RNA sequencing (scRNA-Seq) analyses were performed to measure LGALS3 (i.e. a synonym for Gal3) gene expression in each macrophage of several subtypes present in murine or human plaques.

Results: Preferential binding to M2 macrophages was observed with both AlexaFluor@488-Gal3-F(ab')₂ and ⁸⁹Zr-DFO-Gal3-F(ab')₂ mAbs. Focal and specific ⁸⁹Zr-DFO-Gal3-F(ab')₂ mAb uptake was detected in plaques of ApoE-KO mice by PET/CT. Autoradiography and immunohistochemical analyses of aortas confirmed the expression of Gal3 within plaques mainly in macrophages. Moreover, a specific fluorescent signal was visualized within the lesions of vascular structures burdened by plaques in mice. Gal3 expression in human plaques showed similar Gal3 expression patterns when compared to their murine counterparts.

Conclusions: Our data reveal that ⁸⁹Zr-DFO-Gal3-F(ab')₂ mAb PET/CT is a potentially novel tool to image atherosclerotic plaques at different stages of development, allowing knowledge-based tailored individual intervention in clinically significant disease.

Key words: Atherosclerotic plaques, Inflammation, activated macrophages, PET/CT, Galectin-3

Introduction

Atherosclerosis is a multifactorial chronic inflammatory disorder characterized by a disturbed equilibrium of immune responses and lipid accumulation, leading to plaque development [1]. It is an age-dependent disease and the most common cause of death worldwide [2]. Most atherosclerotic plaques remain clinically asymptomatic, though some undergo a series of changes that cause life-threatening complications [3]. These changes include patches of calcifications, ulcerations associated with shedding of cholesterol emboli into the bloodstream, superimposed thrombosis in areas of plaque fissures, haemorrhage, and aneurysmal dilatations. These changes make plaques vulnerable and prone to events such as myocardial infarction and stroke [4].

Visualization of atherosclerotic plaques and in particular identification of the high-risk lesions prone to rupture *in vivo* is a challenging objective with the ultimate goal to develop pharmacological and/or therapeutic strategies to prevent lethality [5]. Though conventional diagnostic tools yield anatomical and morphological information, they are still of limited value to identify vulnerable plaques and to predict their risk to rupture and subsequent complications [6]. Therefore, to detect vulnerability *in vivo*, imaging approaches are highly relevant to facilitate decisions by the medical community when and how to apply invasive therapies to prevent clinical sequelae of the disease. Molecular imaging offers potential opportunities to develop diagnostic approaches to assess the pathobiology of atherosclerotic plaques. Improved understanding of the molecular and biological processes has stimulated the development of imaging probes, which may aid to identify high-risk atherosclerotic lesions and to apply individually tailored interventions [6]. Since atherosclerosis is a systemic arterial wall disease, molecular imaging of plaques should preferably be performed by whole-body imaging technologies, such as positron emission tomography (PET) imaging.

Monocyte-derived macrophages are major inflammatory cells associated with atherosclerotic lesions and are recognized as key pathophysiologically important immune cells. Therefore, macrophages are gaining attention as imaging targets in atherosclerosis [7-10].

Galectin-3 (Gal3) is a member of the lectin family, which is known to be involved in multiple aspects of inflammatory cell pathology [11]. It is a constitutive marker of activated macrophages [12,13]. Overexpression of Gal3 in the aorta of hypercholesterolemic animals and in human atherosclerotic lesions has been reported, suggesting a direct

involvement of this multifaceted protein in the pathophysiology of the disease [14-16]. Gal3 has therefore been proposed as a potential biomarker for culprit lesions [17]. These characteristics make Gal3 a potential target for non-invasive molecular imaging of atherosclerosis and in particular plaque vulnerability. Radiotracers based on a full Gal3 monoclonal antibody (mAb) and its F(ab')₂ fragment derivative have been developed and used for non-invasive imaging of Gal3-expressing tumors [18-20]. Here, we aimed at investigating whether it is feasible to specifically target and visualize Gal3 expression on the cells present in plaques, *i.e.* subset of macrophages and to a lesser extent other Gal3 positive cell types, using a Gal3-specific probe in apolipoprotein E-knockout (ApoE-KO) mice.

Using zirconium-89 labeled Gal3-F(ab')₂ mAb, we show that nuclear imaging has the potential to visualize specific biological activities associated with plaque progression and/or instability, and that Gal3 expression in atherosclerotic plaques may be used as a novel biomarker to identify patients at high risk of cardiovascular events or to monitor the impact of treatment aimed at plaque stabilization. Using fluorophore coupled Gal3-F(ab')₂ mAb, we delineated the distribution of the probe within the plaques with high resolution, providing initial evidence of the potential sensitivity of the proposed imaging approach.

Methods

Animals

Adult ApoE-KO mice (female, 31-week-old, 29-34 g weight, from Jackson laboratory on the C57BL/6 genetic background) were used for *in vivo* and *ex vivo* imaging studies. Mice were on high fat Western diet (WTD, 21.2% crude fat, E15721-34 from Sniff Spezialdiäten GmbH) for approximately 22 weeks. Age-matched C57BL/6 mice (female, 24-28 g weight, from Charles River Laboratories) were used as controls. Control mice were fed a normal chow diet. Experiments were approved by the local animal care committee (animal license ROB-55.2-2532.Vet_02-17-29.) and were in accordance with the German Animal Welfare Act.

Production of the probes for Gal3 targeting

Gal3-F(ab')₂ mAb was produced by pepsin digestion of a well-characterized rat anti-Gal3-mAb (clone M3/38, Mabtech) binding to an amino-terminal common epitope of human and mouse Gal3 [21]. The digestion was performed after preconditioning of the antibody at acidic pH, as reported earlier [22].

The conjugation with the AlexaFluor488 fluorescent dye and with a Cy5.5-NHS ester

derivative, as well as the conjugation to desferrioxamine (DFO) and radiolabeling with ^{89}Zr was carried out as previously reported (supplementary material) [20].

Selective binding to human macrophages *in vitro*

CD14-positive monocytes were isolated from peripheral blood mononuclear cells (PBMCs) obtained from healthy donors using positive selection technology (MACS technology; Miltenyi Biotec). Successive differentiation in M1 and M2 macrophages was achieved *via* incubation in specific media and in presence of activating substances and cytokines (supplementary material) [23]. Differentiated cells were incubated with 100 nM of AlexaFluor488-Gal3-F(ab')₂ mAb for 1 h at RT. After incubation, media were removed, cells were washed twice with PBS and imaged under a Biorevo BZ-9000 fluorescence microscope (KEYENCE) using a Plan Fluor (Kodak) 20× lens. Another set of cells was incubated with 10 nM of ^{89}Zr -DFO-Gal3-F(ab')₂ mAb for 1 h at RT, or co-incubated with 100-fold excess of unlabelled full-length rat anti Gal3 mAb (clone M3/38, Mabtech, Nacka, Sweden), referred as blocker (supplementary material). After incubation, media were removed, the cells were washed twice with PBS, detached using Macrophage Detachment Solution DXF (C-41330, PromoCell) and transferred into appropriate tubes to measure the associated radioactivity in an automated gamma counter (PerkinElmer 2480 WIZARD²). Data are shown as percentages of cell-associated radioactivity over total radioactivity added. The experiments were performed in triplicate.

In vivo imaging PET/CT

Two groups of mice, ApoE-KO ($n = 12$) and control ($n = 6$), were used for *in vivo* and *ex vivo* imaging. Mice were kept sedated with 1.5-2% isoflurane during injections and PET/CT scans. Static images were acquired 48 h after i.v. injections of ^{89}Zr -DFO-Gal3-F(ab')₂ mAb (2.2 ± 0.2 MBq, 8-9 μg) using the Inveon small animal PET/CT scanner (Siemens, Knoxville, TN, USA) with an acquisition time of 20 min. Images were reconstructed using Siemens Inveon software, which employs a 3-dimensional ordered subsets expectation maximum (OSEM3D) algorithm without attenuation and scatter correction. To confirm tracer uptake specificity, a group of ApoE-KO mice ($n = 3$) was co-injected with a 100-fold excess of unlabeled full-length rat anti Gal3 mAb, and referred as *ApoE-KO blocked*.

Biodistribution and *ex vivo* imaging (PET/CT, autoradiography, and Sudan-IV staining)

Tracer biodistribution and organ accumulation analyses were evaluated as previously described [20]. Whole length aortas (from the sinotubular junction to the iliac bifurcation) were excised under a dissection microscope (Zeiss Stemi DV4 SPOT) as described earlier [23]. Five aortas excised at necropsy from ApoE-KO mice were also scanned *ex vivo* with PET/CT to quantify signal intensity in thoracic and abdominal aorta plaques. Additionally, explanted aortas ($n = 4$ non-blocked, $n = 2$ blocked, and $n = 2$ control) were dissected longitudinally, stained with Sudan-IV for neutral lipids using a previously published method [24,25]. Sudan-IV-stained aortas were then exposed to phosphor imaging plates (FUJI IMAGING PLATE, FUJIFILM), and radioactivity signals were collected for 1 week. The imaging plates were scanned using a phosphor imaging system (Raytest, Straubenhardt, Germany), and the autoradiogram images were analysed for count density. Regions of interest (ROIs) on the whole aorta were used to measure total quantum level units (QL) that were present in that area. Data were used to calculate autoradiographic signal intensity (QL/mm²) in whole aorta.

Fluorescence *in vivo* and *ex vivo* imaging Gal3 expression

Four mice (3 ApoE-KO and 1 control healthy mouse) were sacrificed 48 h after i.v. injection of 100 μg of Cy5.5-Gal3-F(ab')₂ mAb diluted in 300 μl saline solution, embedded in a mixture of Tissue-Tek and black ink (3.2% v/v) inside a cylinder of 4.5 cm diameter, and placed into the -80 °C freezer overnight. Cryosections were obtained using a Leica CM 3500 cryostat (Leica, Wetzlar, Germany) at distances of 20 μm at -17 °C. A highly sensitive fluorescence imaging system was mounted onto the cryostat and macro tissue sections imaged every 5 slices (*i.e.* 100 μm), as reported previously [24-26]. Fluorescence excitation source was a continuous wave (CW) laser diode emitting at 670 nm, while detection was achieved through a 710/10 nm bandpass filter by an iXon electron multiplying charge-coupled device (EMCCD, DV8201-BV, Andor Technology, Belfast, Northern Ireland). Serial sectioning and imaging were fully automated using custom software implemented in LabView (National Instruments, Austin, USA) to control sectioning and trigger image acquisition [27]. Post-processing and visualization were conducted with MATLAB (Mathworks, Natick, USA) and Amira (FEI Visualization Sciences Group, Burlington, USA).

Whole body imaging was performed on 2 ApoE-KO mice and one healthy mouse, while from

the remaining ApoE-KO mouse slices of interest at 10 μm thickness were obtained with a LEICA CM 1950 cryostat. These slices were processed for H&E staining and morphological analyzed with a Zeiss M2 Axio Imager microscope (Carl Zeiss AG, Oberkochen, Germany), while from neighboring unstained slices fluorescent (Cy5.5 filter set; 650/45 nm bandpass filter for excitation and 685 nm longpass filter followed by 720/60 nm bandpass filter for emission) images were captured.

Immunofluorescence staining (IFS) and confocal microscopy

To visualize macrophages, atherosclerotic lesions of the aorta from ApoE-KO mice ($n = 2$) were stained for CD68 and Gal3 as described previously and in supplementary material [28,29]. Secondary antibodies conjugated with Cy5 and Alexa488 were applied. DAPI was used to stain nuclei. Sections were analysed using an SP8 confocal laser scanning microscope (Leica, Mannheim, Germany). For 3D imaging, z-stacks were prepared at 1 μm -intervals with a scan zoom factor of 2 using 100x objective and processed by LasX software (Leica, Mannheim, Germany). ImageJ was routinely used for image processing. All images were saved as TIF files and exported into Adobe Illustrator CS6 for figure arrangement.

Immunohistochemistry analyses for Gal3 expression in murine aortas and human samples

Gal3 expression on murine and human atherosclerotic plaque sections was assessed by immunohistochemistry using a purified horseradish peroxidase-conjugated version of the rat mAb to Gal3 (10 $\mu\text{g}/\text{mL}$; clone M3/38, Mabtech, Sweden) used for the production of the F(ab')₂ [30].

For CD68 and α -SMA staining, mouse anti CD68 (clones PG-M1 and KP-1, Abcam, Cambridge, UK) and mouse anti- α -SMA (Clone 1A4, Dako, Denmark A/S) mAbs were used according to the manufactory instructions at concentrations ranging ~10-30 $\mu\text{g}/\text{mL}$. 4- μm -thick longitudinal cross-sections along the axis of the aorta were prepared from formalin-fixed and paraffin-embedded tissues. For Gal3 immunostaining on human and mouse tissue sections, an antigen retrieval microwave treatment in 0.01 M citrate buffer pH 6.0, at 750 Watt for three cycles (3 minutes each) was applied as previously described [30]. For CD68 and α -SMA immunostaining, heat-induced epitope retrieval was achieved in a solution containing 10 mM Tris-buffer, 1 mM EDTA pH 9.

For indirect immunoperoxidase, mAbs were incubated at 4°C for 30-45 min in a moist chamber.

After washing in PBS the sections were incubated with a secondary goat anti-mouse IgG antiserum-HRP-conjugated (Dako) at dilution 1:200 for 30 min. The enzymatic activity was visualized using 3,3'-diamino-benzidine (Dako, Denmark) as the chromogen.

In order to compare expression of Gal3 in the ApoE-KO model with that in human plaques, 42 surgical samples of human plaques obtained from arteries during surgery (19 women and 23 men) or post-mortem tissues (5 cases), Gal3, CD68 or α -SMA staining were used as described for murine aortas. Images were recorded using an Aperio CS2 ScanScope image capture device (Leica Microsystems, Wetzlar, Germany) and analyzed using Aperio Slide Viewing software (Aperio technologies, CA, USA). Morphological analyses and immunohistochemistry were performed in blind and independently by two experienced pathologists. The study on surgical human samples was carried out according to the ethical guidelines of the Declaration of Helsinki. Specific approval was also obtained from the institutional scientific board and ethical committee of Sant' Andrea Hospital (Prot. CE nr. 8391/2013).

Single cell RNA sequencing (scRNA-Seq) of murine plaque macrophages

Plaques were dissected from aortas of aged (> 78 weeks) ApoE-KO mice ($n = 3$). Plaques were removed using a dissection microscope and cut into small pieces, then digested with enzyme cocktail (400 U/mL collagenase type I, 10 U/mL collagenase type XI, 60 U/mL hyaluronidase and 60 U/mL DNase I, 20 mM HEPES in DPBS) for 40 min at 37°C with slow shaking. Single cell suspensions were stained with fixable viability dye and the panleukocyte marker antibody CD45 (Ebioscience). Total single live CD45⁺ cells were sorted by FACSARIA™ II. The RNA library of total CD45-positive (CD45⁺) live cells was constructed using the Chromium Single Cell 5' Library & Gel Bead Kit (10X Genomics) and sequencing was performed by 26+ 91 bp paired-end next generation sequencing (Illumina). The sequencing raw data was demultiplexed with the cellranger mkfastq pipeline, reads were aligned to mouse mm10 reference transcriptome using STAR alignment built in Cell Ranger (version 3.1.0). All 578 macrophages from total plaque CD45⁺ cells were sub-clustered for 2000 highly expressed genes of each cell using non-linear dimensional reduction (tSNE) algorithm. Three macrophage subtypes were designated following a previous report using marker gene profiles [31]. LGALS3/Gal3 gene expression of each macrophage in murine plaques was shown as violent plots.

scRNA-Seq of human atherosclerotic plaque macrophages

Human plaque single cell sequencing raw data was downloaded from a publicly available databank (<https://figshare.com/s/c00d88b1b25ef0c5c788>; doi: 10.6084/m9.figshare.9206387) [31]. All (1698) macrophages were sub-clustered into three subpopulations by tSNE [32]. Three macrophage populations were defined according to a previous report [31]. LGALS3/Gal3 gene expression of each macrophage subtype in human plaques is shown as violent plots.

Statistics

Data are expressed as means \pm standard deviation (SD). The Mann-Whitney U test was used to compare two variables. A p -value ≤ 0.05 was considered significant. One-way ANOVA was used to compare results from gene sequencing analysis of three independent groups. Statistical analyses were performed using SPSS Statistics software (version 24.0.0, IBM).

Results

Preparation of AlexaFluor488-, Cy5.5-conjugated and ^{89}Zr -DFO-labelled Gal3-F(ab')₂ mAb

The AlexaFluor488-Gal3-F(ab')₂ mAb and Cy5.5-Gal3-F(ab')₂ mAb conjugates showed a fluorochrome/protein ratio of 5.6 ± 0.1 and 3.6 ± 0.1 , respectively. Labelling of DFO-Gal3-F(ab')₂ mAb with ^{89}Zr resulted in a $74 \pm 4\%$ radiochemical yield and a radiochemical purity of $98.5 \pm 0.5\%$ after purification. The specific activity of the probe was 26.0 ± 2.0 MBq/nmol.

AlexaFluor488-Gal3-F(ab')₂ mAb and ^{89}Zr -DFO-Gal3-F(ab')₂ mAb bind to activated human macrophages, mainly M2 (M2a/M2c) subsets *in vitro*

Compared to M0 and M1 macrophages, IL-4/IL-10-activated M2 cells (M2a/M2c) displayed significantly increased uptake of AlexaFluor488-Gal3-F(ab')₂ mAb (Figure 1A). More than 4- and 8-fold greater cell-associated ^{89}Zr -DFO-Gal3-F(ab')₂ mAb radioactivity was observed for M2 (M2a/M2c) macrophages compared to the M1 and M0 subsets, respectively (Figure 1B). Binding of ^{89}Zr -DFO-Gal3-F(ab')₂ mAb to the M2 (M2a/M2c) macrophages was target-specific, as it could be decreased ~ 8 -fold by co-incubation with a 100-fold excess of non-labelled rat anti-Gal3 mAb (Figure 1B).

^{89}Zr -DFO-Gal3-F(ab')₂ mAb accumulates specifically in plaques of ApoE-KO mice

Representative images of PET/CT scans acquired 48 h p.i. with ^{89}Zr -DFO-Gal3-F(ab')₂ mAb for ApoE-KO and control mice are shown in Figure 2A. The lesions in the aortic arch of ApoE-KO mice are clearly visualized *in vivo*. In contrast, no signals were seen in the aortas of control mice. These findings were confirmed by *ex vivo* PET/CT images that showed ^{89}Zr -DFO-Gal3-F(ab')₂ mAb binding in the same area (Figure 2B). Whole body PET/CT and data of the *ex vivo* distribution of ^{89}Zr -DFO-Gal3-F(ab')₂ mAb in ApoE-KO mice are presented in Online Supplementary Figure 1. Atherosclerotic lesions of the abdominal aorta were only faintly detectable *in vivo* due to physiologic uptake of the Gal3 antibody by the liver, but visualized when analyzed *ex vivo* by PET imaging (Figure S2).

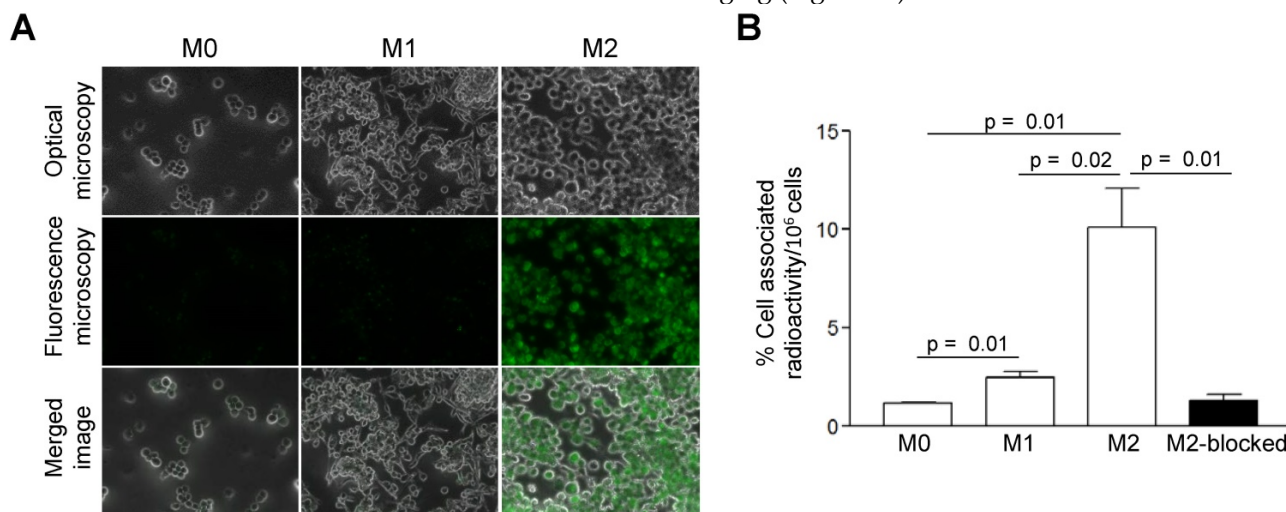


Figure 1. *In vitro* binding-specificity assays. **A**, *In vitro* binding selectivity of AlexaFluor488-coupled Gal3-F(ab')₂ mAb to Gal3 was tested on M0, M1 and M2 (M2a/M2c) polarized macrophages. IL-4/IL-10 activated M2 polarized macrophages displayed significantly enhanced uptake of AlexaFluor488-anti-Gal3-F(ab')₂ when compared with M0 and M1 macrophages. **B**, *In vitro* binding specificity of ^{89}Zr -DFO-Gal3-F(ab')₂ mAb to Gal3 was tested on M0, M1 and M2 (M2a/M2c) polarized macrophages. M2 (M2a/M2c) macrophages in blocked dishes were co-incubated with a 100-fold excess amount of non-labelled full-length anti Gal3 mAb (mean value of three dishes \pm SD). Binding of ^{89}Zr -DFO-Gal3-F(ab')₂ mAb to M2 macrophages was significantly reduced when Gal3 epitopes were saturated with a large molar excess of unlabeled mAb, indicating that binding of ^{89}Zr -DFO-Gal3-F(ab')₂ mAb is specific.

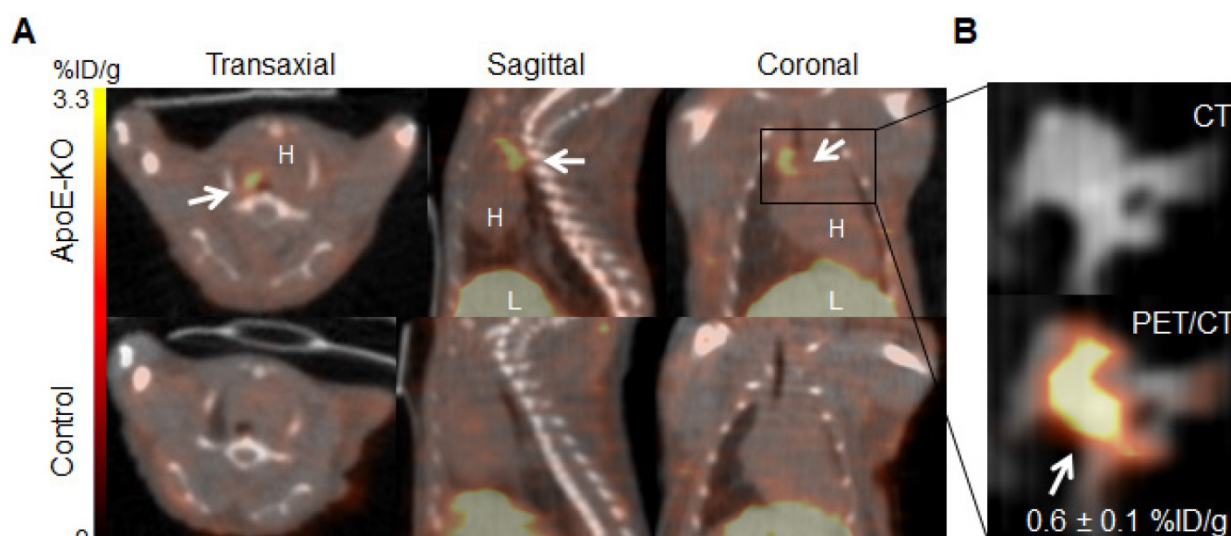


Figure 2. *In vivo* and *ex vivo* PET/CT images. **A**, *in vivo* PET/CT images (axial, sagittal and coronal views) of thorax acquired 48 h post injection of ^{89}Zr -DFO-Gal3-F(ab')₂ mAb from ApoE-KO and control mice. Note the intense focal signal in the first tract of thoracic aorta (white arrows). L stands for liver and H stands for heart. **B**, Corresponding *ex vivo* PET/CT image and *ex vivo* PET signal quantification of the plaque in aortic arch. Scale bar accounts for both images.

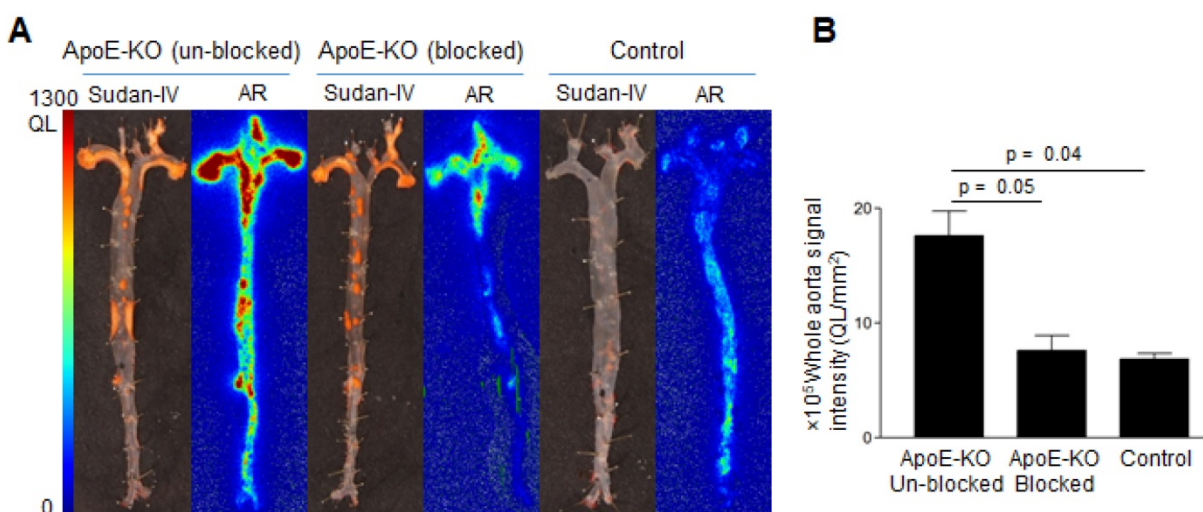


Figure 3. Sudan-IV staining, autoradiography, and autoradiography signal quantification of ^{89}Zr -DFO-Gal3-F(ab')₂ mAb uptake in mice aorta. **A**, Sudan-IV staining and corresponding autoradiography (AR) of aortas excised from ApoE-KO non-blocked, blocked and control mice. **B**, Quantification of the autoradiography images expressed as intensity per unit area of whole aorta (whole aorta autoradiography signal/whole aorta area, QL/mm²). Whole aorta areas were quantified using ImageJ software.

Comparative analysis of Sudan-IV staining and autoradiography of aorta segments showed that the radiolabeled antibody accumulated within atherosclerotic lesions (Figure 3A). Aortas from control mice did not exhibit focal radioactivity signal or lipid staining. Quantification of the autoradiography images showed more than 2-fold greater uptake in aortas of ApoE-KO mice ($(17.6 \pm 3.1) \times 10^5$, QL/mm²) compared to aortic tissue from control mice ($(6.8 \pm 0.8) \times 10^5$, QL/mm²) (Figure 3B). Application of excess unlabeled antibody significantly reduced uptake of radioactivity ($(7.6 \pm 1.8) \times 10^5$ QL/mm², Figure 3B), demonstrating the specificity of Gal3 PET imaging.

Plaque localization via fluorescent imaging

Cryosections of mice which were injected with

Cy5.5-Gal3-F(ab')₂ mAb confirmed accumulation of the Gal3 antibody fragment in atherosclerotic lesions (Figure 4A). This was confirmed by comparing the wide-field fluorescence images to conventional morphology at histology and immunofluorescence (Figure 4B and Figure S3). Despite the low contrast due to tissue autofluorescence and the relative limited dimensions of the regions of interest, a prominent fluorescent signal of different intensities distributed inside the plaques was visualized in all vascular structures with atherosclerotic lesions (Figure 4B insert). These findings provide additional evidence for the sensitivity of the presented imaging approach and will guide future studies to confirm the potential of Gal3 intravascular fluorescent imaging.

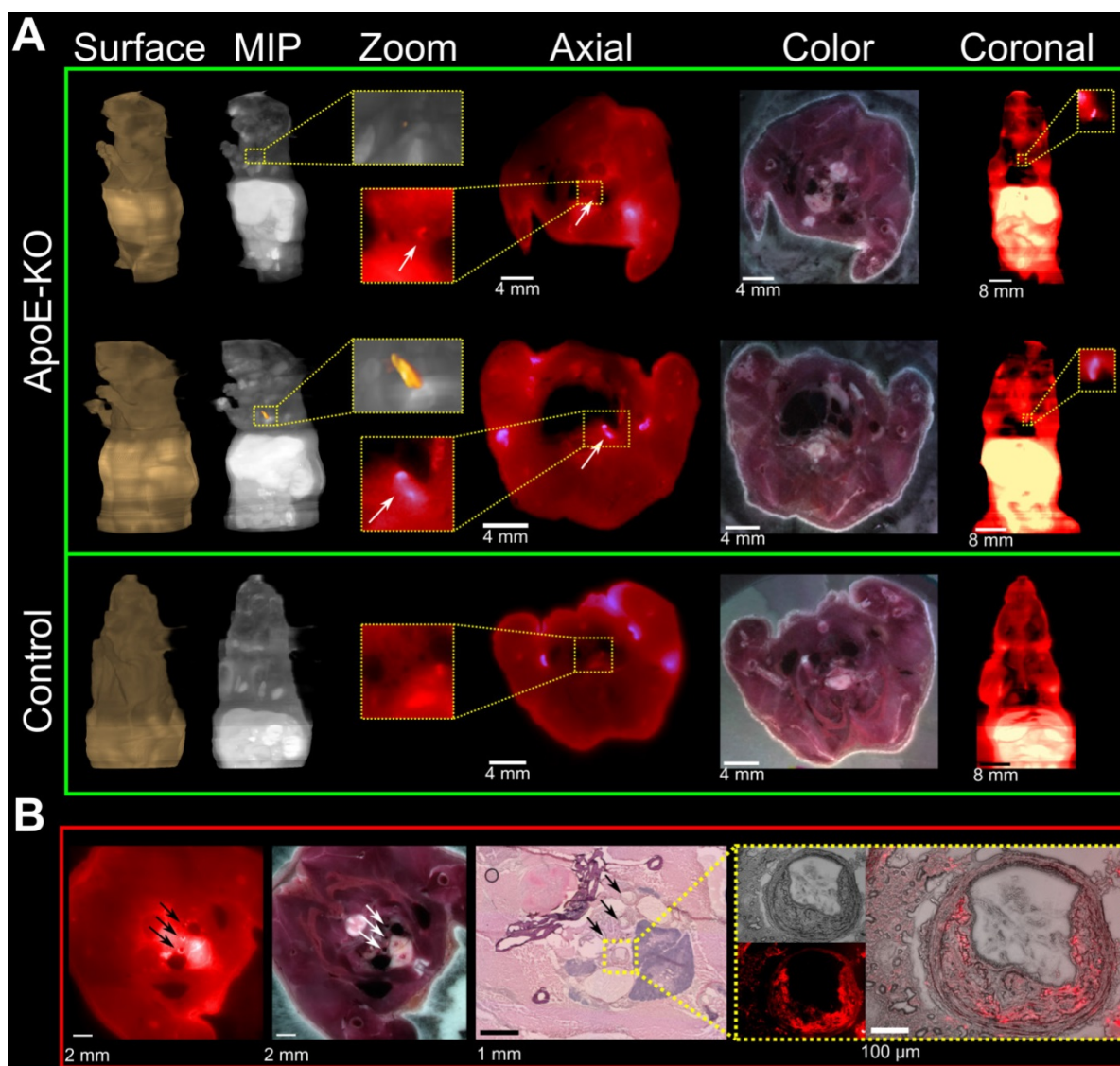


Figure 4. Fluorescence imaging of plaques on serial mouse sections and histopathology confirmation. Three ApoE-KO and one healthy mice were injected with 100 μg of Cy5.5-Gal3-F(ab)² mAb and sacrificed 48 h p.i. **A**, ApoE-KO and control mice were sliced and imaged at a step of 100 μm. Atherosclerotic areas could be confirmed in axial and coronal views, despite the relative low contrast due to autofluorescence signal. MIP: maximum intensity projection. **B**, the accumulation of the tracer in the plaques is further confirmed by H&E staining (middle insert figure) and overlapping fluorescence microscopy obtained from one mouse injected with Cy5.5-Gal3-F(ab)². The external arrows indicate sections of epiaortic vessels originating from the aortic arch, while the middle arrow indicates the initial tract of descending aorta that runs alongside the esophagus. The indicated vascular structures show atherosclerotic lesions with different intensity of fluorescent signal (left image). The blue colored structure under the vascular structures represents the thymus. In the yellow box the common arterial trunk is shown with plaque that causes stenosis (H&E top image, right box). Notably, fusion between H&E and florescent images clearly shows accumulation of the tracer in the plaque, likely due to macrophages infiltration (right box). The fluorescence intensities have been normalized to the corresponding maximum values.

Gal3 expression in murine plaques

Immunohistochemical analyses for Gal3 expression performed on murine aortas revealed strong signals in plaques of the aortic arch, and in both the thoracic and abdominal aorta segments (Figure S4). This finding parallels the radioactive signal visualized via autoradiography analyses (Figure 3) and the *ex vivo* PET imaging of excised aortas (Figure S2 and Figure 5). Immunofluorescence staining showed Gal3 expression by CD68-positive (CD68⁺) macrophages and other myeloid cells located in the fibrous cap layer and shoulder region of plaques (Figure 6 and Figure S5). Gal3 expression

associated with foamy macrophages as well as scattered smooth muscle cells in the arterial wall was noteworthy. Newly formed endothelial cells covering the plaque were also Gal3 positive (Gal3⁺), indicating ongoing involvement of Gal3 in tissue remodeling (Figure 7). These results show that different cell types in diseased arterial walls may express Gal3 though at different levels of intensity.

Gal3 expression in human plaques at different stages of disease progression

Expression of Gal3 was detected in all of 47 human samples at different stages of progression. Lesions with signs of vulnerability showed stronger

Gal3 signals due to the presence of infiltrates of Gal3⁺ foamy macrophages and activated myofibroblasts (Figure S6). Overlapping expression of Gal3 and CD68 confirmed the presence of Gal3⁺ macrophages in the arterial wall. α -SMA-positive (α -SMA⁺) cells including smooth muscle cells, myofibroblasts (cells which produce extracellular matrix components, primarily collagens), scattered foamy macrophages, and some endothelial cells (which are involved in re-endothelization of the plaque) also showed positive signals for Gal3 (Figure 8). It is noteworthy that Gal3 expression analyses were performed on human plaques which were derived from both male and female subjects and did not show apparent gender-dependent differences.

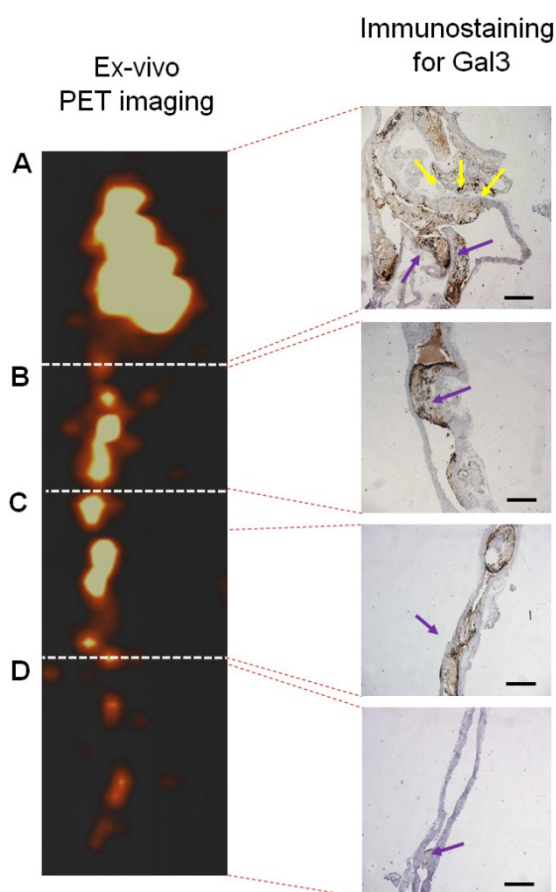


Figure 5. PET signal versus immunohistochemistry staining for Gal3 of a representative aorta excised from ApoE-KO mouse injected with ⁸⁹Zr-DFO-Gal3-F(ab)₂ mAb. Tracer accumulation in different tracts of the aorta was correlating with the brown signal obtained in presence of Gal3 expression in **A**) tract of the origin of aorta with semilunar aortic valve (yellow arrows), which continues with the aortic arch; **B**) tract of thoracic aorta with atherosclerosis lesions (blue arrow); **C**) tract of abdominal aorta with stenotic lesions reach in macrophages (blue arrow); **D**) lumbar aorta presenting slight atherosclerosis (blue arrow). Gal3⁺ macrophages and Gal3 deposition invariably correlate with the signal visualized via PET. Scale bars in IHC images 200 μ m. Magnification 10x.

LGALS3/Gal3 gene expression on murine and human plaque macrophages *in vivo*

Three different macrophage subtypes were

identified in murine plaques: TREM2^{high} macrophages, inflammatory macrophages, and resident-like (Res-like) macrophages. To discriminate TREM2^{high} from resident-like (Res-like) macrophages, the MRC1 (CD11b) gene was utilized as an index marker for M2 macrophages while inflammatory macrophages (M1) were defined by CCR2 gene expression [32]. Using scRNA-seq, we analyzed gene expression profiles of 578 plaque macrophages of aged ApoE-KO mice and 1698 macrophages of human plaques (Figure 9). Our data indicated that both M1 and M2 macrophages express Gal3 transcripts. Yet, a portion of TREM2^{high} M2 macrophages express higher levels of Gal3 transcripts when compared to M1 macrophages both in murine and human plaques *in vivo* (Figure 9A, B). These data support the concept that both M1 and M2 macrophages express Igals3/Gal3 and that the number of these transcripts in a subpopulation of M2 macrophages exceed those in M1 macrophages per cell with statistical significance. Further work is required to identify Igals3/Gal3 transcript and protein expression in other myeloid cells including dendritic cells.

Discussion

Taken together, our findings establish the feasibility of molecular imaging of atherosclerosis by monitoring Gal3 expression on plaques *in vivo* using a PET and fluorescent probe noninvasively. *In vivo* uptake of the antibody fragment was specific for Gal3 expression, as determined by blocking studies. Plaques as small as 3 mm were visualized with high contrast on PET/CT images. At the cellular level, Gal3 immunoreactivity was particularly pronounced in M2 macrophages. Gal3 patterns of expression assessed immunohistochemically in human plaques was similar to the expression pattern evidenced in aortas of the ApoE-KO mice supporting the hypothesis that *in vivo* imaging of the plaques in the murine model can be translated to humans.

Gal3 is a member of the β -galactosyl-binding protein family originally described as cell surface antigen expressed in murine peritoneal macrophages, previously referred to as MAC-2 [33]. Elevated levels of Gal3 in atherosclerosis have been reported to be associated with macrophages [34]. However, the biological role of Gal3 in plaque progression is complex and far from being fully understood [35]. In inflammatory tissue environments, Gal3 modulates inflammation and immune responses possibly contributing to activation of immune cells including lymphocytes and macrophages [36, 37]. Moreover, Gal3 participates in neoangiogenesis, extracellular matrix remodelling and tissue repair [38,39]. Upregulated expression of Gal3 in human

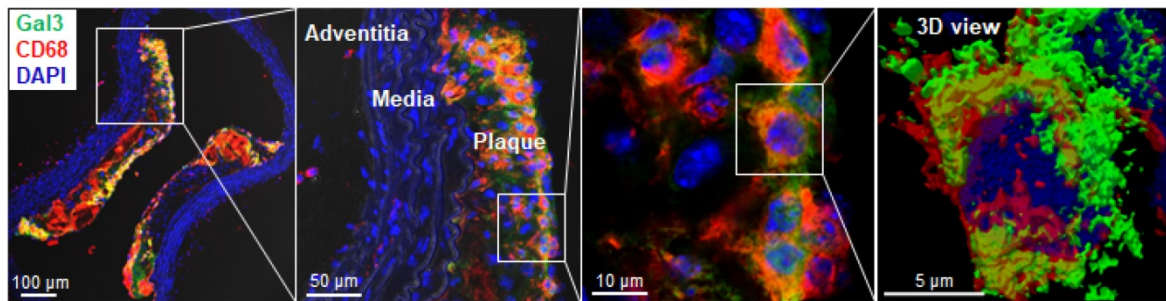


Figure 6. Localization of Gal3 expressing macrophages in plaques via immunofluorescence staining. Immunostaining of Gal3 (green), CD68 (red) in 10µm thick ApoE-KO aorta sections. Gal3⁺CD68⁺ macrophages were mainly located in the fibrous cap and shoulder area of the plaque, but not in the media or adventitia (left). Insets showing higher magnifications and 3D reconstructed maximum intensity projection of z-stacks for co-localized expression of Gal3 and CD68 in plaque shoulder area (middle, left). Overlapping domains of expression are shown in yellow. DAPI stained nuclei are shown in blue.

atherosclerotic lesions was first reported by Nachtigal *et al.* in plaque specimens obtained from autopsies of trauma victims. In those specimens, Gal3 localized predominantly in macrophages and foam cells and its level of expression correlated with plaque burdens [15, 40]. Moreover, Papaspyridonos *et al.* reported that human Gal3 expression is marked in unstable regions of the plaques with high cellularity including foamy macrophages, collagen-producing myofibroblasts, activated newly formed endothelial cells and lipid deposits [16]. In view of these data it is conceivable that Gal3 plays clinically relevant roles in atherosclerosis.

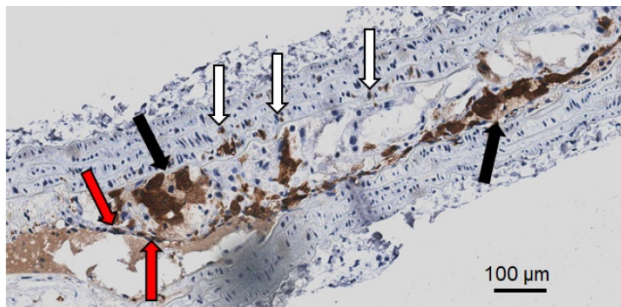


Figure 7. Representative picture showing different Gal3⁺ cells in a large plaque in 4 µm thick ApoE-KO aorta section. In dark brown (black arrows) Gal3 is visible in foamy macrophages that preferentially express Gal3 in the cytoplasm. Other foamy macrophages are faintly positive or negative at immunohistochemistry in the observed clusters. Scattered smooth muscle cells in the arterial muscular wall also express Gal3 (white arrows). Neofomed endothelial cells covering the plaque are also Gal3 positive (red arrows). This picture shows that different cell types in plaques may express Gal3. The proportion of these cell types is variable in each plaque. Magnification 20x.

Our observations support the hypothesis that plaques harbor several Gal3⁺ cell types of the diseased arterial wall with preferential expression in polarized macrophages though other immune cells, as well as SMCs and endothelial cells also seem to be involved. Fibrous and sclerotic plaques, which are more stable and show scarce cellularity, do not appear to express high levels of Gal3. Novak *et al.* have compared intra- and extracellular expression profiles of Gal3 in classically (M1) and alternatively activated macrophages, and found that Gal3 expression was

significantly higher in M2 macrophages with respect to the classically activated cells *in vitro* [13]. Our *in vitro* binding results on macrophage subpopulations are consistent with these observations, and show approximately 3-fold higher uptake of ⁸⁹Zr-DFO-Gal3-F(ab')₂ mAb on M2 (M2a/M2c) macrophages as compared to non-activated and classically activated cells. Moreover, scRNA-seq analyses of plaque-resident macrophages indicate that a portion of TREM2^{high} M2 macrophages express higher level of lgals3/Gal3 transcripts when compared to M1 macrophages both in murine and human plaques. These data indicate that Gal3-F(ab')₂ mAb-based tracers preferentially bind to M2 macrophages. However, the pathological role of alternative macrophages in atherosclerosis progression and their contribution to plaque (in)stability remains to be fully understood [41-49]. Indeed, there is recent evidence for pro-atherogenic properties of alternative macrophages that were previously thought to be anti-atherogenic [44-48]. Alternative macrophages may represent important contributors to plaque progression and instability by producing matrix metalloproteinase-9 (MMP-9), which is capable of degrading type IV collagen and triggering plaque rupture [46-49]. Yet, ApoE/Gal3 double-KO mice were reported to develop significantly lower numbers of lesions when compared with ApoE-KO mice [50]. In a similar study performed by Mackinnon *et al.*, deletion of Gal3 in ApoE-KO mice was associated with smaller plaques with reduced necrotic cores and collagen content [51]. More work is needed to clarify the conundrum of pro- versus anti-atherosclerotic impacts of Gal3 in different biological contexts such as age, sex and risk factor burdens [52].

Different experimental imaging approaches, like ultrasound molecular imaging (USI), fluorescent imaging, intravascular photoacoustic imaging, magnetic resonance imaging (MRI) associated to experimental probes have been studied for this purpose [53-56].

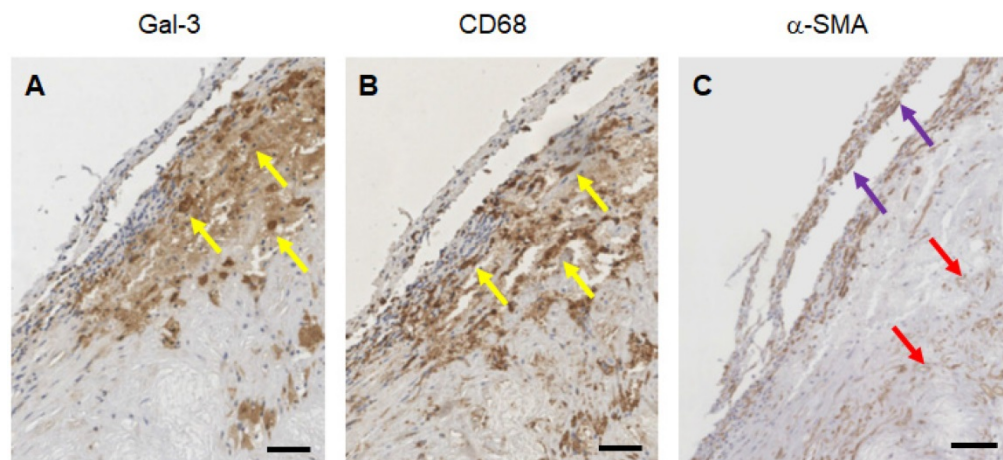


Figure 8. Immunostaining of human plaques for Gal3, CD68 and α -SMA expression. A representative panel of immunohistochemical analyses of a large plaque of human aorta is shown. **A)** Gal3 immunostaining using rat mAb to Gal3 clone M3/38 shows positive cells in an atherosclerotic lesion. Some of the cells appear dark-brown, others are faintly stained suggesting different expression level of the lectin protein. **B)** CD68 immunostaining (mAb PG-M1) of the same lesion shows an overlapping signal, which is consistent with a macrophage phenotype (yellow arrows). **C)** α -SMA staining indicate smooth spindle cells (myofibroblast), microvessels and scattered macrophages (see the foamy cytoplasm of some positive cells at the base of the picture, red arrows). Some of these cells express Gal3. Scale bars 200 μ m. Magnification 10x.

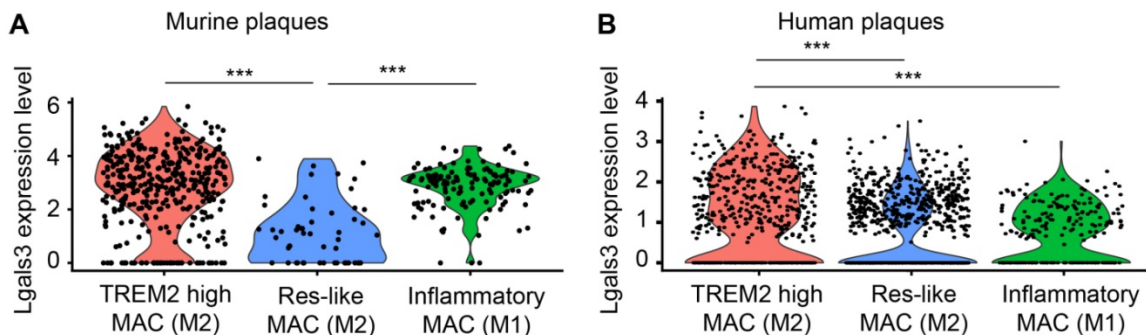


Figure 9. LGALS3/Gal3 gene expression in plaque macrophages in vivo. **A)** Single cell sequencing of plaque-derived macrophages of aged ApoE-KO mice revealed LGALS3 gene on three macrophage populations *in vivo*. Each dot represents one individual cell. One-way ANOVA, $n = 392$ TREM2 high macrophages (TREM2 high MAC), $n = 54$ tissue resident-like macrophages (Res-like MAC), $n = 134$ inflammatory macrophages. $***P < 0.001$. **B)** Single cell sequencing of human plaque macrophages revealed LGALS3/Gal3 gene on three macrophage populations *in vivo*. Each dot represents one individual cell. One-way ANOVA, $n = 520$ TREM2 high MAC, $n = 963$ Res-like MAC, $n = 215$ inflammatory macrophages. $***P < 0.001$.

Different PET and single photon emission computed tomography (SPECT) radiotracers have been investigated for imaging of plaques [6, 23, 45, 57-59]. Among them, Fluorine-18 fluorodeoxyglucose (^{18}F -FDG) has become a mainstay of metabolic imaging in atherosclerosis [57, 60]. However, the uptake of ^{18}F -FDG by macrophages is unspecific and it is taken up by the same membrane transporters that take up glucose in all metabolically active cells. In addition, this approach has limitations in the specific setting of vascular imaging, including physiological uptake in the left ventricular myocardium that impairs imaging of coronary arteries, interaction with blood glucose metabolism, and the need for an extended fasting period before imaging. Due to the high affinity of ^{18}F -fluoride to inorganic hydroxylapatite and its ability to localize noninvasively in bone metastasis or soft tissue dystrophic calcification, ^{18}F -sodium fluoride (^{18}F -NaF)-PET has also been investigated as a potential noninvasive imaging methodology to identify calcified tissue deposits in plaques with high-risk characteristics [61, 62]. By

comparing ^{18}F -NaF versus ^{18}F -FDG in cancer patients, Derlin and co-workers reported contrasting results about accumulation of both tracers in calcified lesions, with colocalization of ^{18}F -NaF and ^{18}F -FDG occurring in only 6.5% of the arterial lesions studied [63]. Considering that not all plaques show calcifications and not all vascular sites of inflammation demonstrate ^{18}F -NaF uptake, it has been suggested that fluoride uptake probably occurs in dying foam cells, or in the senescent, dying, foam cells when cell metabolism is reduced or absent [64]. These aspects represent intrinsic limitations of this imaging methodology. Experimental probes which bind to receptors expressed on macrophages, like the mannose receptor, have also been investigated [23, 45, 56]. The major limitation of these probes lies in the restricted expression of mannose receptors in macrophages. To the best of our knowledge, mannose receptors are not expressed by other cell types involved in plaque remodeling.

The main advantage of using ^{89}Zr -DFO-Gal3-F(ab')₂ mAb over above mentioned tracers is that our

probe binds specifically and with high sensitivity to major actors of plaque evolution and vascular repair. This methodology may therefore allow real time imaging of different phases of plaque maturation.

Some limitations associated with the current study require further considerations. First, due to typical late imaging time points and extended patient radiation exposure, the clinical use of an ^{89}Zr -labeled F(ab')₂ fragment for studying plaques could be challenging. To overcome this problem, production of a chimeric/human F(ab') anti-Gal3 mAb with optimized plasma half-life for clinical usage is in progress in our laboratory. Second, the fluorescent dye which was used to label Gal3-F(ab')₂ mAb was primarily used to study the intra-plaque distribution of the antibody fragment with higher resolution, which is not achievable by autoradiography. Intravascular fluorescence molecular imaging (FMI) is an emerging technology that enables imaging of specific molecular events within rupture-prone plaques [65]. Our results support the important possibility that Gal3 expression-imaging may qualify to distinguish stable versus unstable plaques using intravascular FMI, after labeling antibody fragments with near-infrared fluorescent dyes having a longer emission wavelength, such as indocyanine green (ICG) [66].

The role of Gal3 in physiological and pathophysiological processes has led to several distinct galectin inhibitors, both for experimental purposes and potential clinical use as novel therapeutics [67-69]. Such inhibitors could be potentially useful to modulate activation of macrophages or other cell types present in plaques. A tracer specific for Gal3 targeting would be of considerable interest to monitor the response to novel therapeutic approaches.

In conclusions, our findings indicate that PET imaging of plaques by targeting Gal3 appears to be feasible. Clinical translation of these imaging approaches holds promise to improve the management of patients affected by plaques at high risk of lethal clinical outcomes of the disease.

Abbreviations

Gal3: Galectin-3; DFO: desferrioxamine-thioureyll-phenyl-isothiocyanate; ^{89}Zr : zirconium-89; Fab'2: Fragment antigen-binding-2; (ApoE-KO) mice: apolipoprotein E knockout mice; CD68: cluster of differentiation 68 (a monocyte/macrophage marker); α -SMA: alpha-smooth muscle actin; Cy5.5-NHS: cyanine 5.5 succinimidyl ester; AlexaFluor488-NHS: alexafluor488 succinimidyl ester; PET/CT: positron emission tomography/computer tomography; FMT: fluorescence molecular tomography; H&E:

Hematoxylin and eosin staining; HRP: horseradish peroxidase; scRNA-Seq: single cell RNA sequencing; TREM2: Triggering receptor expressed on myeloid cells 2; Res-like macrophages: resident-like macrophages; LGALS3: lectin, galactoside-binding, soluble, 3 gene; ^{18}F -NaF: ^{18}F -sodium fluoride; ^{18}F -FDG: ^{18}F -fluorodeoxyglucose; ICG: indocyanine green; intravascular FMI: intravascular fluorescent molecular imaging.

Supplementary Material

Supplementary figures and tables.

<http://www.thno.org/v11p1864s1.pdf>

Acknowledgements

Sources of Funding

This research has been supported by Deutsches Zentrum für Herz-Kreislauf-Forschung e.V. (DZHK) and by Deutsche Forschungsgemeinschaft (DFG) grants: DA 1552/2-1 and (CRC 824/3 2017; subproject C10) granted to CD and (CRC 824/3 2017; subproject Z3) granted to VN. AB is supported by AIRC (The Italian Association for Cancer Research). Single cell sequencing data were supported by DFG grants: YI 133 /3-5, HA 1083/15-5 and Ha 1083/17-1.

Disclosures

Armando Bartolazzi has ownership of a patent regarding the use of radiolabeled antibodies for Gal3 imaging *in vivo* (patent no. 1388763, Italy). All other authors have nothing to declare.

Competing Interests

The authors have declared that no competing interest exists.

References

- van Varik BJ, Rennenberg RJ, Reutelingsperger CP, Kroon AA, de Leeuw PW, Schurgers LJ. Mechanisms of arterial remodeling: lessons from genetic diseases. *Front Genet.* 2012; 3: 290.
- Benjamin EJ, Muntner P, Alonso A, Bittencourt MS, Callaway CW, Carson AP et al. Heart disease and stroke statistic-2019 Update: a report from the American Heart Association. *Circulation.* 2019; 139: e56-e528.
- Grimm JM, Schindler A, Freilinger T, Cyran CC, Bamberg F, Yuan C, et al. Comparison of symptomatic and asymptomatic atherosclerotic carotid plaques using parallel imaging and 3 T black-blood *in vivo* CMR. *J Cardiovasc Magn Reson.* 2013; 15-44.
- Ward MR, Pasterkamp G, Yeung AC, Borst C. Arterial remodeling. Mechanism and clinical implications. *Circulation.* 2000; 102: 1186-91.
- Wildgruber M, Swirski FK, Zernecke A. Molecular imaging of inflammation in atherosclerosis. *Theranostics.* 2013; 3: 865-84.
- Bucerius J, Dijkgraaf I, Mottaghy FM, Schurgers LJ. Target identification for the diagnosis and intervention of vulnerable atherosclerotic plaques beyond ^{18}F -fluorodeoxyglucose positron emission tomography imaging: promising tracers on the horizon. *Eur J Nucl Med Mol Imaging.* 2019; 46: 251-265.
- Gerrity RG, Naito HK, Richardson M, Schwartz CJ. Dietary induced atherogenesis in swine. Morphology of the intima in prelesion stages. *Am J Pathol.* 1979; 95: 775-92.
- Swirski FK, Nahrendorf M. Leukocyte behaviour in atherosclerosis, myocardial infarction, and heart failure. *Science.* 2013; 339: 161-166.
- Sager HB, Nahrendorf M. Inflammation: a trigger for acute coronary syndrome. *Q J Nucl Med Mol Imaging.* 2016; 60: 185-193.
- Quillard T, Libby P. Molecular imaging of atherosclerosis for improving diagnostic and therapeutic development. *Circ Res.* 2012; 111: 231-244.

11. Dumic J, Dabelic S, Flögel M. Galectin-3: an open-ended story. *Biochim Biophys Acta*. 2006; 1760: 616-635.
12. Kim K, Mayer EP, Nachtigal M. Galectin-3 expression in macrophages is signaled by Ras/MAP kinase pathway and up-regulated by modified lipoproteins. *Biochim Biophys Acta*. 2003; 1641: 13-23.
13. Novak R, Dabelic S, Dumic J. Galectin-1 and galectin-3 expression profiles in classically and alternatively activated human macrophages. *Biochim Biophys Acta*. 2012; 1820: 1383-1390.
14. Nachtigal M, Legrand A, Sasiela W, Watson SD, Fowler SD. Gene expression in macrophage foam cells of carrageenan-induced granulomas in hypercholesterolemic rabbits. *FASEB J*. 1994; 8: A393.
15. Nachtigal M, Al-Assaad Z, Mayer EP, Kim K, Monsigny M. Galectin-3 expression in human atherosclerotic lesions. *Am J Pathol*. 1998; 152: 1199-1208.
16. Papaspyridonos M, McNeill E, de Bono JP, Smith A, Burnand KG, Channon KM, et al. Galectin-3 is an amplifier of inflammation in atherosclerotic plaque progression through macrophage activation and monocyte chemoattraction. *Arterioscler Thromb Vasc Biol*. 2008; 28: 433-440.
17. Yu L, Ruifrok WP, Meissner M, Bos EM, van Goor H, Sanjabi B, et al. Genetic and pharmacological inhibition of galectin-3 prevents cardiac remodeling by interfering with myocardial fibrogenesis. *Circ Heart Fail*. 2013; 6: 107-17.
18. Bartolazzi A, D'Alessandria C, Parisella MG, Signore A, Del Prete F, Lavra L, et al. Thyroid cancer imaging in-vivo by targeting the anti-apoptotic molecule galectin-3. *PLoS One*. 2008; 3: e3768.
19. D'Alessandria C, Braesch-Andersen S, Bejo K, Reder S, Blechert B, Schwaiger M, et al. Noninvasive in-vivo imaging and biologic characterization of thyroid tumors by ImmunoPET targeting of Galectin-3. *Cancer Res*. 2016; 76: 3583-3592.
20. De Rose F, Braeuer M, Braesch-Andersen S, Otto AM, Steiger K, Reder S, et al. Galectin-3 targeting in thyroid orthotopic tumors opens new ways to characterize thyroid cancer. *J Nucl Med*. 2019; 60: 770-776.
21. Inohara H, Raz A. Functional evidence that cell surface galectin-3 mediates homotypic cell adhesion. *Cancer Res*. 1995; 55: 3267-3271.
22. Rousseaux J, Rousseaux-Prevost R, Bazin H. Optimal conditions for the preparation of Fab and F(ab)2 fragments from monoclonal IgG of different rat IgG subclasses. *J Immunol Methods*. 1983; 64: 141-146.
23. Varasteh Z, Mohanta S, Li Y, Lopez Armbruster N, Braeuer M, Nekolla SG, et al. Targeting mannose receptor expression on macrophages in atherosclerotic plaques of apolipoprotein E-knockout mice using ⁶⁸Ga-NOTA-anti-MMR nanobody: non-invasive imaging of atherosclerotic plaques. *EJNMMI Res*. 2019; 9: 5.
24. Wang H, Willershäuser M, Karlas A, Gorpas D, Reber J, Ntziachristos V, et al. A Dual Ucp1 Reporter Mouse Model for Imaging and Quantitation of Brown and Brite Fat Recruitment. *Mol Metab*. 2019; 20: 14-27.
25. Napp J, Markus MA, Heck JG, Dullin C, Möbius W, Gorpas D, et al. Therapeutic Fluorescent Hybrid Nanoparticles for Traceable Delivery of Glucocorticoids to Inflammatory Sites. *Theranostics*. 2018; 8: 6367-6383.
26. Schottelius M, Wurzer A, Wissmiller K, Beck R, Koch M, Gorpas D, et al. Synthesis and Preclinical Characterization of the PSMA-targeted Hybrid Probe PSMA-I&F for Nuclear and Fluorescence Imaging of Prostate Cancer. *J Nucl Med*. 2019; 60: 71-78.
27. Symvoulidis P, Perez CC, Schwaiger M, Ntziachristos V, Westmeyer GG. Serial sectioning and multispectral imaging system for versatile biomedical applications. In 2014 IEEE 11th International Symposium on Biomedical Imaging (ISBI), 2014; 890-893.
28. Mohanta S, Yin Ch, Weber Ch, Hu D, Habenicht A. Aorta Atherosclerosis Lesion Analysis in Hyperlipidemic Mice. *Bio Protoc*. 2016; 6: e1833.
29. Hu D, Mohanta SK, Yin C, Peng L, Ma Z, Srikakulapu P, et al. Artery tertiary lymphoid organs control aorta immunity and protect against atherosclerosis via vascular smooth muscle cell lymphotoxin beta receptors. *Immunity*. 2015; 42:1100-1115.
30. Bartolazzi A, Gasbarri A, Papotti M, Bussolati G, Lucante T, Khan A, et al. Application of an immunodiagnostic method for improving preoperative diagnosis of nodular thyroid lesions. *Lancet*. 2001; 357: 1644-1650.
31. Fernandez DM, Rahman AH, Fernandez NF, Chudnovskiy A, Amir ED, Amadori L, et al. Single-cell immune landscape of human atherosclerotic plaques. *Nat Med*. 2019; 25: 1576-1588.
32. Cochain C, Vafadarnejad E, Arampatzi P, Pelisek J, Winkels H, Ley K, et al. Single-cell RNA-Seq reveals the transcriptional landscape and heterogeneity of aortic macrophages in murine atherosclerosis. *Circ Res*. 2018; 122: 1661-1674.
33. Ho MK, Springer TA. Mac-2, a novel 32,000 Mr mouse macrophage subpopulation-specific antigen defined by monoclonal antibodies. *J Immunol*. 1982; 128: 1221-8.
34. Gao Z, Liu Z, Wang R, Zheng Y, Li H, Yang L. Galectin-3 Is a Potential Mediator for Atherosclerosis. *J Immunol Res*. 2020; 2020: 5284728.
35. Suthahar N, Meijers WC, Silljé HHW, Ho JE, Liu FT, de Boer RA. Galectin-3 activation and inhibition in heart failure and cardiovascular disease: An Update. *Theranostics*. 2018; 8: 593-609.
36. Rabinovich GA, Toscano MA. Turning "sweet" on immunity: galectin-glycan interactions in immune tolerance and inflammation. *Nat Rev Immunol*. 2009; 9: 338-52.
37. Toscano MA, Bianco GA, Ibarregui JM, Croci DO, Correale J, Hernandez JD, et al. Differential glycosylation of TH1, TH2 and TH-17 effector cells selectively regulates susceptibility to cell death. *Nat Immunol*. 2007; 8: 825-34.
38. Elola MT, Ferragut F, Méndez-Huergo SP, Croci DO, Bracalente C, Rabinovich GA. Galectins: Multitask signaling molecules linking fibroblast, endothelial and immune cell programs in the tumor microenvironment. *Cell Immunol*. 2018; 333: 34-45.
39. Li T, Zha L, Luo H, Li S, Zhao L, He J, et al. Galectin-3 mediates endothelial-to-mesenchymal transition in pulmonary arterial hypertension. *Aging Dis*. 2019; 10: 731-745.
40. Lee YJ, Koh YS, Park HE, Lee HJ, Hwang BH, Kang MK, et al. Spatial and temporal expression, and statin responsiveness of galectin-1 and galectin-3 in murine atherosclerosis. *Korean Circ J*. 2013; 43: 223-30.
41. Finn AV, Saeed O, Virmani R. Macrophage Subsets in Human Atherosclerosis. *Circ Res*. 2012; 110: 110.
42. Chinetti-Gbaguidi G, Staels B. Response to the Letter by Finn et al. *Circ Res*. 2012; 110: e65-e66.
43. Chinetti-Gbaguidi G, Baron M, Bouhrel MA, Vanhoutte J, Copin C, Sebti Y, et al. Human atherosclerotic plaque alternative macrophages display low cholesterol handling but high phagocytosis because of distinct activities of the PPARγ and LXRα pathways. *Circ Res*. 2011; 108: 985-95.
44. Mauriello A, Servadei F, Sangiorgi G, Anemona L, Giacobi E, Liotti D, et al. Asymptomatic carotid plaque rupture with unexpected thrombosis over a non-canonical vulnerable lesion. *Atherosclerosis*. 2011; 218: 356-362.
45. Tahara N, Mukherjee J, de Haas HJ, Petrov AD, Tawakol A, Haider N, et al. 2-deoxy-2-[18F]fluoro-D-mannose positron emission tomography imaging in atherosclerosis. *Nat Med*. 2014; 20: 215-219.
46. Tziakias DN, Lazarides MK, Tentis IK, Georgiadis GS, Eleftheriadou E, Chalikias GK, et al. Gelatinases [matrix metalloproteinase-2 (MMP-2) and MMP-9] induce carotid plaque instability but their systemic levels are not predictive of local events. *Ann Vasc Surg*. 2005; 19: 529-533.
47. Jager NA, Wallis de Vries BM, Hillebrands JL, Harlaar NJ, Tio RA, Slart RHJA, et al. Distribution of Matrix Metalloproteinases in Human Atherosclerotic Carotid Plaques and Their Production by Smooth Muscle Cells and Macrophage Subsets. *Mol Imaging Biol*. 2016; 18: 283-291.
48. Sapienza P, di Marzo L, Borrelli V, Sterpetti AV, Mingoli A, Piagnerelli R, et al. Basic fibroblast growth factor mediates carotid plaque instability through metalloproteinase-2 and -9 expression. *Eur J Vasc Endovasc Surg*. 2004; 28: 89-97.
49. Pourcet B, Staels B. Alternative macrophages in atherosclerosis: not always protective! *J Clin Invest*. 2018; 128: 910-912.
50. Nachtigal M, Ghaffar A, Mayer EP. Galectin-3 Gene Inactivation Reduces Atherosclerotic Lesions and Adventitial Inflammation in ApoE-Deficient Mice. *Am J Pathol*. 2008; 172: 247-255.
51. MacKinnon AC, Liu X, Hadoke PW, Miller MR, Newby DE, Sethi T. Inhibition of galectin-3 reduces atherosclerosis in apolipoprotein E-deficient mice. *Glycobiology*. 2013; 23: 654-663.
52. Di Gregoli K, Somerville M, Bianco R, Thomas AC, Frankow A, Newby AC, et al. Galectin-3 identifies a subset of macrophages with a potential beneficial role in atherosclerosis. *Arterioscler Thromb Vasc Biol*. 2020; 40: 1491-1509.
53. Yan F, Sun Y, Mao Y, Wu M, Deng Z, Li S, et al. Ultrasound Molecular Imaging of Atherosclerosis for Early Diagnosis and Therapeutic Evaluation through Leucocyte-like Multiple Targeted Microbubbles. *Theranostics*. 2018; 8: 1879-1891.
54. Choi JY, Ryu J, Kim HJ, Song JW, Jeon JH, Lee DH, et al. Therapeutic effects of targeted PPARγ activation on inflamed high-risk plaques assessed by serial optical imaging *in vivo*. *Theranostics*. 2018; 8: 45-60.
55. Wang Y, Chen J, Yang B, Qiao H, Gao L, Su T, et al. *In vivo* MR and fluorescence dual-modality imaging of atherosclerosis characteristics in mice using proflin-1 targeted magnetic nanoparticles. *Theranostics*. 2016; 6: 272-86.
56. Ma S, Motevalli SM, Chen J, Xu MQ, Wang Y, Feng J, et al. Precise theranostic nanomedicines for inhibiting vulnerable atherosclerotic plaque progression through regulation of vascular smooth muscle cell phenotype switching. *Theranostics*. 2018; 8: 3693-706.
57. Sun ZH, Rashmizal H, Xu L. Molecular imaging of plaques in coronary arteries with PET and SPECT. *J Geriatr Cardiol*. 2014; 11: 259-73.
58. Kim EJ, Kim S, Seo HS, Lee YJ, Eo JS, Jeong JM, et al. Novel PET imaging of atherosclerosis with ⁶⁸Ga-labeled NOTA-neomannosylated human serum albumin. *J Nucl Med*. 2016; 57: 1792-1797.
59. Varasteh Z, Hyafil F, Anizan N, Diallo D, Aid-Launais R, Mohanta S, et al. Targeting mannose receptor expression on macrophages in atherosclerotic plaques of apolipoprotein E-knockout mice using ¹¹¹In-tilmancept. *EJNMMI Res*. 2017; 7: 40.
60. Rudd JH, Hyafil F, Fayad ZA. Inflammation imaging in atherosclerosis. *Arterioscler Thromb Vasc Biol*. 2009; 29: 1009-16.
61. Mitterhauser M, Toegel S, Wadsak W, Mien LK, Eideherr H, Kletter K, et al. Binding studies of [18F]fluoride and polyphosphonates radiolabelled with [99mTc], [111In], [153Sm] and [188Re] on bone compartments: verification of the pre vivo model? *Bone*. 2005; 37: 404-12.
62. Derlin T, Richter U, Bannas P, Begemann P, Buchert R, Mester J, et al. Feasibility of 18F-sodium fluoride PET/CT for imaging of atherosclerotic plaque. *J Nucl Med*. 2010; 51: 862-5.
63. Derlin T, Tóth Z, Papp L, Wisotzki C, Apostolova I, Habermann CR, et al. Correlation of inflammation assessed by 18F-FDG PET, active mineral deposition assessed by 18F-fluoride PET, and vascular calcification in atherosclerotic plaque: a dual-tracer PET/CT study. *J Nucl Med*. 2011; 52: 1020-7.

64. Nakahara T, Dweck MR, Narula N, Pisapia D, Narula J, Strauss HW. Coronary Artery Calcification: From Mechanism to Molecular Imaging. *JACC Cardiovasc Imaging*. 2017; 10: 582-593.
65. Khraishah H, Jaffer AF. Intravascular molecular imaging to detect high-risk vulnerable plaques: current knowledge and future perspectives. *Current Cardiovascular Imaging Reports*. 2020; 13: 8.
66. Bertrand MJ, Abran M, Maafi F, Busseuil D, Merlet N, Mihalache-Avram T, et al. In-vivo near-infrared fluorescence imaging of atherosclerosis using local delivery of novel targeted molecular probes. *Sci Rep*. 2019; 9: 2670.
67. Delaine T, Cumpstey I, Ingrassia L, Le Mercier M, Okechukwu P, Leffler H, et al. Galectin-inhibitory thiodigalactoside ester derivatives have antimigratory effects in cultured lung and prostate cancer cells. *J Med Chem*. 2008; 51: 8109-14.
68. Blanchard H, Yu X, Collins PM, Bum-Erdene K. Galectin-3 inhibitors: a patent review (2008-present). *Expert Opin Ther Pat*. 2014; 24: 1053-65.
69. Johannes L, Jacob R, Leffler H. Galectins at a glance. *J Cell Sci*. 2018; 131: jcs208884.